THE JOURNAL OF PHYSICAL CHEMISTRY C
A JOURNAL OF THE AMERICAN CHEMICAL SOCIETY

pubs.acs.org/JPCC
Article

Universal Radiative Lifetimes in the Long-Lived Luminescence of Si Quantum Dots

Tomáš Popelář, Pavel Galář, Filip Matějka, Giacomo Morselli, Paola Ceroni, and Kateřina Kůsová*

Cite This: J. Phys. Chem. C 2023, 127, 20426−20437
Read Online

ABSTRACT: Silicon quantum dots (SiQDs) represent a perspective light emitting material. Here, we show that their typical long-lived photoluminescence can be fully radiative. However, despite the fully radiative nature, the overall yield of light emission from SiQDs is still hindered by dark QDs, the understanding of which is only very limited so far. To address this problem, first, we experimentally quantify the dependence of radiative lifetimes on the emission photon energy and show that this dependence is universal across different types of samples and different laboratories. Second, we use this dependence to quantify the internal photoluminescence quantum yield using simply the emission-photon energy dependence of measured photoluminescence (PL) lifetimes as the input. The knowledge of the internal quantum yield then lets us determine the relative population of dark SiQDs if the external quantum yield is known. The application of our approach to the decoupling of the influence of nonradiative processes and dark quantum dots can be easily applied by other researchers, which will shed more light on the mechanism of PL quenching in dark QDs. Besides focusing on dark QDs, we observe that the PL decays of SiQDs can be non-single-exponential despite being fully radiative and suggest the natural variation of radiative lifetimes as a possible mechanism responsible for the non-single-exponential character of PL decay. Lastly, we emphasize the importance of average lifetimes as the quantity characterizing PL decays, especially in the case of non-single-exponential PL decays in the absence of a generally accepted physical model explaining the PL dynamics.

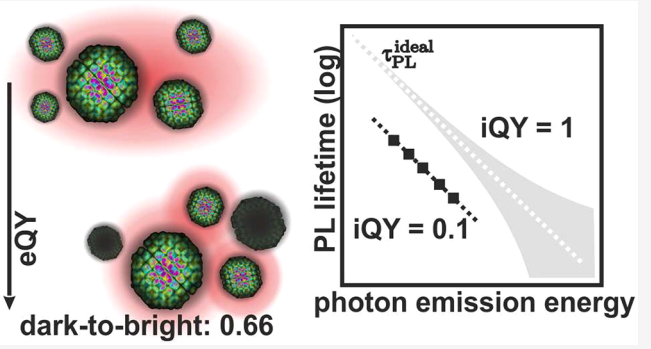

1. INTRODUCTION

Silicon quantum dots (SiQDs) are a class of materials attractive due to their relative nontoxicity and material abundance.[1−4] Compared to their bulk counterpart, they feature promising light-emitting properties, which predetermine them for use in solar energy conversion as QD-based luminescent solar concentrators,[5,6] in electronic devices, therapeutic biomedicine[7] and medical imaging.[8] Despite the general consensus about the important role the quantum confinement effects play in the light emission process,[9−14] some of the aspects of SiQD photoluminescence (PL) are still being disputed[15,16] and various processes influencing or determining PL properties are still being proposed for consideration.[17−22] SiQDs passivated with oxide or long alkyl chains exhibit nearly universally size-tunable PL with slow non-single-exponential decay spectrally located in the red and near-infrared spectral region,[2,23] sometimes accompanied by a blue-shifted faster component.[14,24,25] The question as to why, in SiQDs, the observed PL decay almost always deviates from the expected single-exponential character, occurring for example in direct-bandgap QDs, is still a subject of debate.[18,26−29]

In terms of potential optical applications of QDs, two quantities are of paramount importance: the PL decay time τ_{PL} characterizing how fast the absorbed excitation energy is released and the photoluminescence quantum yield (efficiency), which is related to the efficiency with which the absorbed energy can be extracted in the form of light. In general, τ_{PL} can be divided into lifetimes corresponding to the radiative and nonradiative pathways:

$$\frac{1}{\tau_{PL}} = \frac{1}{\tau_r} + \frac{1}{\tau_{nr}} \quad (1)$$

where τ_r and τ_{nr} are the radiative and the nonradiative lifetime, respectively. Whereas τ_{PL} can easily be determined from a time-resolved PL measurement, the separation of τ_{PL} into the radiative and nonradiative parts is nontrivial. The correct way to deduce the radiative lifetimes is by "directly" exploiting the Purcell effect,[30−32] which describes the influence of the local environment around the QD on τ_{PL}. A modulation of the environment (local density of states), for example by

Received: August 10, 2023
Revised: September 21, 2023
Published: October 4, 2023

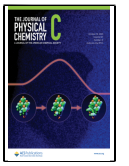

https://doi.org/10.1021/acs.jpcc.3c05423
J. Phys. Chem. C 2023, 127, 20426−20437

depositing a metal layer with variable thickness onto the active SiQD thin film[30] or by using a curved mirror,[33] leads to the modulation of the radiative part of τ_{PL} while the nonradiative part remains unaltered. In this way, the radiative and nonradiative parts can be separated.

On the other hand, the quantum yield is a more nuanced quantity. Most of the time, the so-called external quantum yield (eQY), which characterizes an ensemble of QDs, is measured. Precise measurements of eQY (η_E) are performed using an integrating sphere setup,[34,35] where the number of emitted photons N_{em} is compared to the number of the absorbed photons N_{abs}:

$$\eta_E = \frac{N_{em}}{N_{abs}} \tag{2}$$

QYs of the very first SiQDs were quite low, just a few percent, but in SiQDs fabricated by more modern techniques, values of η_E as high as[14] 68% are being reported. With the exception of several elaborate experiments,[36] eQY is commonly reported as an emission-wavelength independent value characterizing the whole emission spectrum.

On the level of an individual QD, the quantity of interest is its internal quantum yield (iQY):

$$\eta_I^j = \frac{\tau_{PL}^j}{\tau_r^j} \tag{3}$$

where the superscript j refers to the photoluminescence and radiative lifetimes of a particular QD. It is tempting to consider the external and internal quantum yields of eq 2 and eq 3 the same, to determine the radiative lifetime using a measured η_E and τ_{PL} as $\tau_r = \tau_{PL}/\eta_E$[37,38] and then to interpret the macroscopic measured τ_{PL} and the calculated τ_r as the photoluminescence and radiative lifetimes of a "typical" QD, respectively. However, this approach is almost always incorrect because it hinges on the assumption that all the QDs in the ensemble are exactly, or at least roughly, the same in terms of their η_I^j. Almost every QD sample contains the so-called dark QDs, which absorb excitation, but emit basically no PL ($\eta_I^{dark} = 0$).[32,39] These dark QDs obviously significantly differ from the light-emitting ones in terms of their η_I^j, implying that the simple approach to the separation of the radiative and nonradiative pathways in the PL decay cannot be used.

The radiative lifetime τ_r is an important quantity because it describes the optical performance of an ideal QD system in which nonradiative pathways are negligible. The nonradiative recombination pathways and the presence of dark QDs are then characteristics of a particular sample, which are the decisive factor determining how much the PL performance of that sample deviates from the idealized behavior. Therefore, the separation of the individual factors deteriorating the PL QY in an SiQD sample is an important step in the optimization of PL performance. Unfortunately, such separation is an extremely complex experimental task that cannot be done routinely on a sample-to-sample basis.

In this article, we focus mostly on the long-lived emission of SiQDs ($\tau_{PL}^{slow} \approx 100\ \mu s$), whereas the fast component ($\tau_{PL}^{fast} \approx 10$ ns), which can sometimes be detected,[14,24,25] is mentioned only briefly. We observe, using detailed PL characterizations of various SiQD samples as well as literature data, that the radiative lifetimes in the long-lived emission of SiQDs are a universal material characteristic shared by SiQDs fabricated by completely different techniques. To the best of our knowledge, the idea of radiative lifetimes as a generally valid material characteristic in SiQDs has not yet been addressed experimentally, despite the clear utility and importance of such an observation. We quantify the dependence of the radiative lifetimes on the emission photon energy or rather on the corresponding emission wavelength λ (for simplicity, these two terms are used interchangeably throughout this article). Our analysis can now serve as a tool for the decoupling of the nonradiative pathways and the relative population of dark SiQDs in other samples, using experimentally relatively simple measurements of QY and spectrally and temporally resolved PL. The observed universal $\tau_r(\lambda)$ dependence well follows a single-exponential curve over a wide range of emission photon energies, as is expected for an effect resulting from quantum confinement. It also strongly indicates that the long-lived PL in many colloidal SiQDs is fully radiative despite the clear non-single-exponential character of the PL decay. The non-single-exponential character is confirmed by a simple data-quality measure that we introduce. This measure helps us quantify the extent to which noise influences the determination of the PL decay shape. Moreover, we propose the idea that this commonly reported non-single-exponential character of PL decay typical for SiQDs can arise also from a variation of radiative lifetimes in the ensemble.

2. METHODS

2.1. Sample Fabrication. *2.1.1. Nonthermal Plasma Synthesis (NTP-SiQDs).* SiQDs were synthesized in a non-commercial flow-through glass reactor with low-pressure nonthermal plasma as detailed elsewhere.[40] The output source power was set to 150 W. The PL wavelength of the sample was tuned by changing the composition of the synthesis gas ((i) 80 sccm of silane in Ar with 10 sccm of H_2, (ii) 80 sccm of silane in Ar with 50 sccm of H_2, and (iii) 40 sccm of silane, 40 sccm of Ar, and 100 sccm of hydrogen). The estimated residence time of the forming nanoparticles in the plasma was about 15 ms. The synthesis times ranged from 3 to 5 min. In the oxidized samples (NTP:SiQDs:O), the sample was collected on a glass substrate placed 10 cm below the aperture in the form of dry powder and allowed to naturally oxidize under ambient conditions. For subsequent hydrosilylation (NTP:SiQDs:C), a collector was attached to a special adapter for the in-liquid sample collection. A standard glass vial with an inner diameter of 1.25 cm filled with 5 mL of dodecene (Sigma-Aldrich, 95%) was used as the collector device, and the dodecene dispersion with collected SiQDs was ultrasonicated for 15 min. The vial was then placed on a hot plate with an aluminum heating nest. The temperature was set at 200 °C, and the samples were stirred for 8−11 h while stirring. The temperature of the samples was monitored with an FLIR camera. The sample was purified using two centrifugation/precipitation cycles in an ethanol/hexane solvent/antisolvent pair, dispersed, and kept in toluene.

2.1.2. Disproportionation of Hydrogen Silsequioxane (HSQ-SiQDs). SiQDs were synthesized following the protocols published elsewhere.[41] In brief, the synthesis was based on the thermal disproportionation of hydrogen silsequioxane (HSQ) and the SiQDs were subsequently HF-etched, yielding free-standing H-terminated particles. These were then alkyl-capped by hydrosilylation in the presence of 1-dodecene and initiated with diazonium salt, leading to the dodecene-capped QDs (HSQ-SiQDs:C). The diameter of HSQ-SiQDs:C was about 4 nm.

https://doi.org/10.1021/acs.jpcc.3c05423
J. Phys. Chem. C 2023, 127, 20426−20437

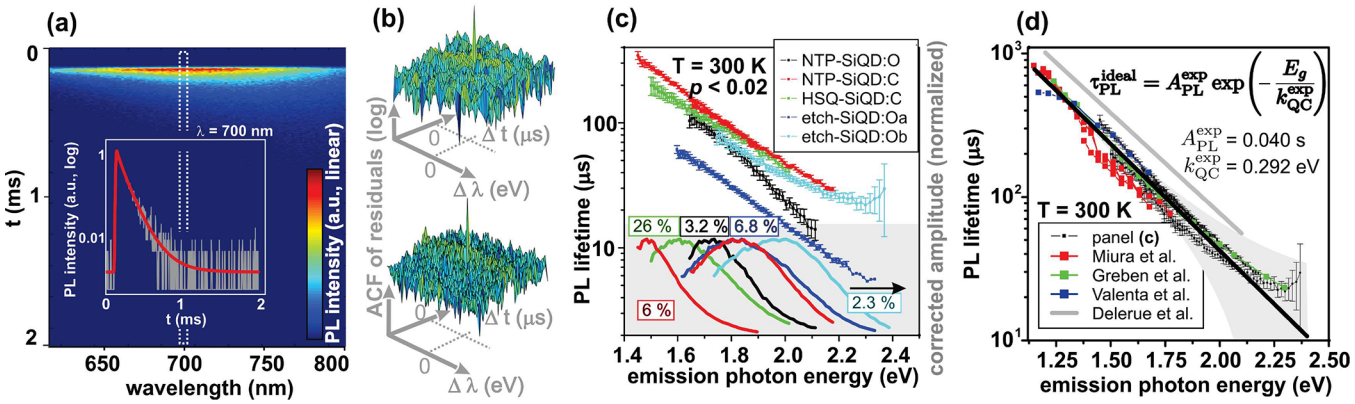

Figure 1. (a) Example of a photoluminescence map $I(t, \lambda)$ with a selected fitted PL decay as an inset. (b) Two examples of a quality-of-fit assessment using an autocorrelation function (ACF) of residuals for a lower (top, 10^{24} photons/scm^2) and higher (10^{25} photons/scm^2) excitation intensity. (c) Average PL lifetimes τ_{PL} as a function of photon emission energy for differently prepared samples from Table 1, extracted from measurements analogous those in panel a. The fit ambiguity parameter p from eq S8 introduced later in the text ensures that only high-quality data are included. The bottom part of the panel presents the corresponding PL spectra and measured eQYs. (d) Selected data sets (in gray) from panel c compared to PL decays reported as fully radiative in the literature by Miura et al.,[30] Greben et al.,[28] and Valenta et al.[32] plotted as the average lifetime τ_{PL}. These data were fitted to obtain an ideal $\tau_{PL}^{ideal}(\lambda)$ curve as noted in the panel (the black line with 66% prediction bands in gray). Theoretical calculations of radiative rates by Delerue et al.[48] are also included.

Table 1. List of the Studied Samples and Measured Quantum Yields[a]

label	preparation	treatment	eQY (%)	A_{PL} (s)	D
NTP-SiQD:O	nonthermal plasma synthesis	natural oxidation	3.2	0.037	
NTP-SiQD:C	nonthermal plasma synthesis	hydrosilylation with 1-dodecene	6.0	0.048	15
HSQ-SiQD:C	thermal disproportionation of HSQ	hydrosilylation with 1-dodecene	26	0.033	3
etch-SiQD:Oa	electrochemical etching of Si wafers	natural oxidation	6.8	0.0068	2
etch-SiQD:Ob	electrochemical etching of Si wafers	natural oxidation, deagglomeration	2.3	0.029	40

[a]The A_{PL} parameter characterizes the weight of the slow non-radiative pathways (eq 7) and the D parameter the relative proportion of dark QDs (eq 10), as explained in the text. The A_{PL} parameter of the first sample is determined only for the lower emission photon energy range (≈ 1.6−1.8 eV), where the slope of the dependence of lifetime on the emission photon energy does not significantly deviate from the ideal value.

2.1.3. Electrochemical Etching (etch-SiQDs). SiQDs prepared by electrochemical etching are in detailed described elsewhere.[42] In brief, the preparation is based on the electrochemical etching of B-doped p-type wafers in HF:EtOH solution, following the "standard" and "white" conditions.[42] After etching, the on-wafer layer of SiQDs was intensely rinsed in pure ethanol EtOH and dried in air ("standard", denoted etch-SiQDs:a here) or underwent further treatment in H_2O_2 ("white", etch-SiQDs:b). The resulting SiQD layer was mechanically scraped-off the substrate, and SiQDs were aged under ambient atmosphere and then dispersed in EtOH. For the deagglomeration procedure[43] (etch-SiQDs:b), SiQDs were treated in a high power ultrasonic ethanoic bath (absorbed energy 100 kJ, 1 s on and 1 s off pulses). The mean diameter of etch-SiQDs was around 2.5−3 nm.

2.2. Optical Characterization. The time-resolved spectra were recorded by a streak camera Hamamatsu C10627 (with best time resolution of 15 ps) after excitation by a femtosecond laser PHAROS (150 fs pulses, Light Conversion) or a nanosecond laser NL 302 (5 ns pulses, Ekspla). The excitation wavelength was selected in the range 315−630 nm by nonlinear interactions in a harmonics generator HiRO or an optical parametric amplifier ORPHEUS, both by Light Conversion. All of the spectra were corrected for the setup spectral sensitivity. The QYs were measured by the absolute method (integrating sphere setup) following the procedure described by Valenta et al.[34] where the LEDs were replaced by the laser-driven light source (EQ-99X, Energetiq) coupled to the 15 cm monochromator (Acton SP 2150i, Princeton Instruments) as the excitation source.

2.3. Data Analysis. The analysis of the data is based on the procedure outlined elsewhere.[44] In short, the PL measurements are made as a function of wavelength and they are transformed into emission photon energies in eVs including the $1/\lambda^2$ spectral correction factor.[45] The emission-photon-energy dependent series of PL decays $I(\lambda, t)$ is then fitted using a convolution of a Gaussian curve and a PL decay function. The Gaussian curve represents the laser pulse as measured by the detection system or the instrumental response function. Its characteristics are known and fixed in the fit because they had been determined prior to the measurement of PL. Thus, a set of λ dependent characterizations of the fit ($\tau_{SE}(\lambda)$ and $\beta(\lambda)$) and the spectral profile $I_0(\lambda)$ can be obtained from one PL map. The normalization of the decay function (e.g., the stretched-exponential) at each λ to unity ensures that the value of $I_0(\lambda)$ corresponds to the integrated PL intensity at the particular λ. Thus, $I_0(\lambda)$ represents the spectrum of the corresponding PL component.

The quality of the fit is assessed using multiple approaches. In addition to common approaches, we plot the data and the fitted decay curve in offset logarithmic scale,[44] where the vertical scale is logarithmic, but a small constant (typically equal the smallest value) is added to the vertical scale before applying the logarithm so that all the values are positive. This procedure ensures that all the data are visible in the plot because simple semilogarithmic plots omit zero and negative

https://doi.org/10.1021/acs.jpcc.3c05423
J. Phys. Chem. C 2023, 127, 20426−20437

data, skewing the visual information present in the figure. This procedure is useful for assessing the accuracy of the fit in the tail of the PL decay data. Moreover, we calculate the autocorrelation function of residuals[46,47] and plot it in a logarithmic vertical scale (see Figure 1b). If the autocorrelation function is flat, then there is no underlying trend of a deviation between the data and the fit, which implies that the model describes the data very well.

3. RESULTS AND DISCUSSION

3.1. Slow PL Decay in Differently Synthesized SiQDs. We used a set of SiQD samples fabricated by three different methods with two different types of surface passivation; for details, see Section 2.1. The studied SiQDs were (i) synthesized in nonthermal plasma (NTP-SiQDs), (ii) synthesized by annealing of an Si-rich SiO_x precursor and subsequently extracted from the matrix (HSQ-SiQDs), or (iii) fabricated by a top-down approach by electrochemical etching of a monocrystalline Si wafer (etch-SiQDs).[42] The SiQD samples were then either oxidized under ambient conditions for at least a month (SiQDs:O) and dispersed in a solvent or were surface-terminated by hydrosilylation with 1-dodecene and purified (SiQDs:C). This set of samples listed in Table 1 underwent a series of time-resolved PL measurements using pulsed laser excitation and a detection with the camera coupled to a spectrograph to produce spectrally and temporally resolved PL maps $I(t, \lambda)$ as shown in Figure 1a. These PL maps represent a series of emission-wavelength/emission-photon-energy dependent PL decays $I_\lambda(t)$ and as such can be used to deduce the emission-photon-energy dependent PL lifetime $\tau_{PL}(\lambda)$ and the corresponding PL spectrum $I_0(\lambda)$. The bandgap (HOMO−LUMO energy) of these SiQDs is tuned by their size through quantum confinement effects.[12,49] Therefore, disregarding a possible influence of line-width broadening,[27,28] which is indeed negligible for a wide spectral range, the $\tau_{PL}(\lambda)$ dependence can be viewed as a representation of the corresponding size dependence of the QD's bandgap by substituting $\tau_{PL}(d)$ for $\tau_{PL}(d(\lambda))$. Since the correct determination of the size distribution in an ensemble of SiQDs is a complicated task,[21] we will use the bandgap-energy $\tau_{PL}(\lambda)$ representation throughout this article for the sake of simplicity.

The observed PL decays $I(t, \lambda)$ are universally stretched-exponential (see also further discussion in Section 3.5)

$$I(t, \lambda) = I_0(\lambda) \exp\left\{-\left(\frac{t}{\tau_{SE}(\lambda)}\right)^{\beta(\lambda)}\right\} \quad (4)$$

where t is time and $\tau_{SE}(\lambda)$ and $\beta(\lambda)$ are the stretched-exponential lifetime and dispersion parameter, respectively. While these two quantities, frequently used to quantitatively describe experimental observations, are often treated and discussed separately,[26,27,37] we characterize our samples using the intensity averaged lifetime[29] τ_{PL} instead (for more details, see Section S2). The important feature of averaged lifetimes is their ability to characterize the whole PL decay independently of the applied mathematical model, be it a stretched-exponential or a combination of two or more exponentials, provided that the fit is of high quality.[28,50] For the case of the most common stretched-exponential decay shape from eq 4, the averaged lifetime τ_{PL} can be calculated simply by inserting the τ_{SE} and β parameters directly into[29]

$$\tau_{PL} = \frac{\Gamma(2/\beta)}{\Gamma(1/\beta)}\tau_{SE} \quad (5)$$

where $\Gamma()$ is the gamma function.

The average lifetimes $\tau_{PL}(\lambda)$ extracted from the measured PL maps are presented in Figure 1c. We emphasize here that we applied a procedure[44] which ensures that our analysis is free of artifacts, as explained in detail in Section S3. The adequacy of the characterization of the PL tail and the background is also judged, among other ways, by visualizing the autocorrelation function of residuals (ACF) in Figure 1b, which should be flat for a good data-to-fit correspondence. Importantly, we verified that the lifetimes $\tau_{PL}(\lambda)$ obtained in this way are robust as they are independent of many experimental conditions, including excitation intensity (10^{24}−10^{26} ph/cm^{2}s), mode of excitation (femtosecond or nanosecond laser), and excitation wavelength (315−400 nm, two-photon or two-step excitation). One subtle deviation from the $\tau_{PL}(\lambda)$ behavior is suggested by a small peak in the ACF for higher excitation intensity measurements (see the bottom ACF in Figure 1b) around $\Delta t \approx 0$ μs, hinting at a possible much faster component most likely connected with Auger recombination.[51]

3.2. Purely Radiative Lifetimes. In Figure 1c, four of the $\tau_{PL}(\lambda)$ data sets fall on a very similar curve when plotted as the average lifetime τ_{PL} rather than the more common τ_{SE} parameter from eq 4. In general, the measured lifetime τ_{PL} is determined by the lifetimes corresponding to both the radiative and nonradiative channels (eq 1). Thus, there are two ways to attain the same $\tau_{PL}(\lambda)$: (i) either the variation of τ_r and τ_{nr} across the different types of samples coincidentally cancels itself out or (ii) the nonradiative pathways are negligible $\tau_{nr} \to \infty$ and the measured lifetimes are in fact purely radiative $\tau_{PL} \approx \tau_r$. Thus, a question arises as to what the radiative lifetimes of these samples are. In slowly emitting SiQD colloids, a determination of radiative lifetimes directly in the colloid is especially demanding,[28] because measurements based on Purcell effect would require local modulation of the effective refractive index of the medium surrounding the QD, in this case the liquid itself. Such a modulation could in principle be realized, for example, by means of optical interference, but the contrast of the optically induced modulation in a liquid would very likely be too low to allow for a meaningful analysis of the signal. To the best of our knowledge, up to now, iQY of colloidal SiQDs had been quantified only in specially engineered samples with much shorter radiative lifetimes and thus much higher signal levels and the measurements were performed after the SiQDs had been deposited on a substrate, not directly in the colloid.[33] In slowly emitting matrix-embedded SiQDs, in which well-defined layers are generally easier to form and where the properties of the surrounding medium can be modulated by physically shaping the sample, iQY measurements were successfully reported.[30,32,52] Specifically, our literature search revealed three reports on radiative lifetimes in matrix-embedded SiQDs,[30,32,52] two reports on fully radiative PL decay in colloidal SiQDs[27,28] and one report on radiative lifetimes in colloidal SiQDs.[37] The report on radiative lifetimes of colloidal SiQDs by Liu et al.[37] is automatically excluded, because its methodology to obtain the radiative lifetimes is the over-simplified recalculation of photoluminescence lifetimes as described in the introductory section instead of a rigorous application of the Purcell effect approach, which renders the obtained values invalid. Out of the remaining reports, one

https://doi.org/10.1021/acs.jpcc.3c05423
J. Phys. Chem. C 2023, 127, 20426−20437

measurement of radiative lifetimes by Kalkman et al.[52] and one report on fully radiative lifetimes in colloidal SiQDs by Sangghaleh et al.[27] were excluded as outliers because the reported values were detectably lower than in the rest of the data sets. One set of data by Miura et al.[30] needed to be recalculated into the averaged lifetime values due to reporting the traditional τ_{SE} and two of the reports by Valenta et al.[32] and Greben et al.,[28] which already use the averaged lifetimes notation, applied long-pulsed excitation conditions. The long-pulse excitation is known to yield longer lifetime values[53] and thus the behavior reported in these two studies was extrapolated to the commonly applied short-pulse excitation conditions to simplify the comparison with literature data. For more details on the compilation of these literature data, see Section S1.

Now, to test the second possibility of our measured lifetimes from Figure 1c being radiative, we use (i) these reported literature data on measured *radiative* lifetimes[30,32] of matrix-embedded SiQDs, (ii) the reported fully radiative PL lifetimes of colloidal SiQDs, all of which were gathered independently on samples nominally similar to ours, and (iii) our matching $\tau_{PL}(\lambda)$ curves. We compare all these data sets in Figure 1d. Given the typical error involved in the measurements of radiative lifetimes (at least ±10%),[52] the reported radiative lifetimes of SiQDs are remarkably similar to our measured ones. This very good match of completely independent data supports the claim that several types of our SiQDs have τ_{PL}'s indeed very close to the purely radiative values.

Purely radiative lifetimes imply close-to-unity iQY (eq 3). The occurrence of purely radiative microsecond PL decay in colloidal SiQDs is not as surprising as it might seem at first sight due to several factors. First, as a result of SiQDs' long radiative lifetimes, the most common competitive nonradiative channels potentially lowering iQY, linked for example to core-surface interfacial defects, will be orders of magnitude faster, and thus, they would, if present, shorten the observed τ_{PL} significantly, basically rendering it fast or completely quenched. Second, despite the similarities, colloidal SiQDs differ from SiQDs embedded in a matrix. In a SiQD/matrix system, excited carriers can be trapped within the matrix around the SiQD, giving rise to additional slower ($\tau_r \approx \tau_{nr}$) nonradiative channels,[32] which can lower the iQY below 1, but still to a value high enough to be measurable. In accordance with the proposed scenario, high, but lower than unity, iQYs were reported in matrix-embedded SiQDs (0.77,[52] 0.7−1,[30] and ∼0.8[32]). Moreover, in analogy to our results, the reports of radiative lifetimes of matrix-embedded SiQDs confirm that the corresponding radiative lifetimes are well-matched among the individual samples[30] and it is only the weight of the nonradiative channel that varies. Therefore, in colloidal SiQDs, where the slow relaxation pathway of the excited carriers is not additionally complicated by the presence of the matrix, purely radiative PL decay is fully plausible.

3.3. Influence of Quantum Confinement. The quantification of the matching lifetime dependence for different SiQD samples is depicted in Figure 1d, where the dependence is fitted with an exponential[48]

$$\tau_r^{ideal} = A_{PL} \exp(-E_g/k_{QC}) \quad (6)$$

Here, E_g represents the bandgap (or the corresponding HOMO−LUMO energy). The $1/k_{QC}$ slope parameter describing the relationship between the photon emission energy and the corresponding radiative lifetime is a proxy parameter for the strength of quantum confinement, or in other words, for the influence of the quantum confinement effects (size d) on the radiative lifetimes (the inverse of radiative rates). This experimentally determined trend is quantitatively the same in differently fabricated types of samples, which confirms the universality of this fundamental property, implying that SiQDs are influenced by quantum confinement to the same extent. Notably, the theoretically predicted k_{QC}^{th} parameter using a tight-binding technique including the phonon modes and averaging over a wide range of QD sizes yields[48] a value very similar to ours: k_{QC}^{exp} = 0.2917 ± 0.0539 eV compared to k_{QC}^{th} = 0.31 eV.

Typical experimentally acquired PL spectra of SiQDs span a broad range of emission photon energies (see Figure 1d), which, in addition to the existence of size dispersion, implies that the λ dependence of potential nonradiative lifetimes is often not, in terms of its trend, much stronger than that of the radiative ones; otherwise, the nonradiative pathways would overwhelm the radiative ones and very little or no PL would be observable. This line of reasoning has been confirmed by the direct decoupling of the emission photon energy dependence of the radiative and nonradiative lifetimes in matrix-embedded SiQDs using the Purcell effect published elsewhere by Valenta et al.[32] Thus, within the spectral range of reasonably efficient light emission, the slope of the measured $\tau_{PL}(\lambda)$ for a nonideal sample involving also slow nonradiative pathways might not be much different from the ideal $1/k_{QC}^{exp}$. For example, the fitted quantum-confinement parameter of the etch-SiQD:Oa sample is very close to the ideal value of k_{QC}^{exp} ($k_{QC}^{etch\text{-}SiQD:Oa}$ = 0.288 eV). However, a potential deviation of measured $\tau_{PL}(\lambda)$ from the ideal $1/k_{QC}^{exp}$ slope over only a certain range of photon energies implies that a certain size range of SiQDs has a worse PL performance. In our measurements, such underperformance occurs for oxidized plasma-synthesized SiQDs emitting at shorter wavelengths, that is those with smaller sizes. However, if the same samples undergo hydrosilylation instead of oxidation, the deviation disappears. This observation suggests that natural oxidation of small plasma-synthesized SiQDs very likely negatively impacts their PL performance.

In addition to the $1/k_{QC}$ slope, the τ_{PL} dependence also includes the A_{PL} offset parameter. Similarly to $1/k_{QC}^{exp}$, also the offset parameter quantified in this article based on experiments is only slightly lower than the theoretically predicted value[48] (A_{PL}^{exp} = 0.0400 ± 0.0003 s and A_{PL}^{th} = 0.05 s), as confirmed by the comparison of the experimental and theoretical curves in Figure 1d. When quantified in a sample involving nonradiative microsecond processes such as the etch-SiQD:Oa sample in Figure 1b, this parameter gives an indication about the relative importance of the microsecond nonradiative pathways, as explained in Section S4. In our measurements, the lower A_{PL} parameter is found for the etch-SiQD:Oa sample, which is understandable, because in standard etched SiQDs, a high degree of agglomeration of the individual SiQDs occurs.[43] The agglomeration of SiQDs held together by a SiO_2 tissue enables the same nonradiative relaxation mechanisms of trapping in the material surrounding the SiQD core which occur in matrix-embedded SiQDs.

3.4. Determination of Nonradiative Lifetimes of the Slow Component. In reality, the determination of the A_{PL} parameter from the experimental data might not be entirely straightforward. The value of the quantum-confinement parameter k_{QC}^{exp} as determined in Figure 1d is robust and is

https://doi.org/10.1021/acs.jpcc.3c05423
J. Phys. Chem. C 2023, 127, 20426−20437

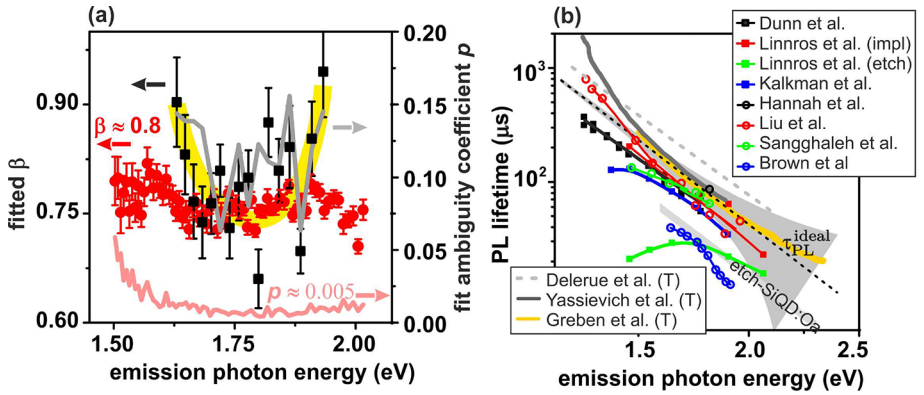

Figure 2. (a) Fitted β parameter for the PL decays of the HSQ-SiQD:C sample under lower (10^{24} photons/cm^2, black and gray) and higher (10^{27} photons/cm^2, red and pale red) excitation intensity. The two $\tau_{PL}(\lambda)$'s corresponding to these two measurements both follow the dependence from Figure 1d. The gray and pale red segmented lines represent the fit ambiguity coefficients p from eq S8 for the two data sets, respectively. Please note how a higher p correlates with a higher fitted β. The thick yellow curve serves as a guide-for-the-eye of how the presented dependence could be perceived for the data set in black. (b) Comparison of the ideal lifetime dependence τ_{PL}^{ideal} with literature data. Oxidized SiQD samples are shown as solid squares, and hydrosilylated, as open circles. Literature data include reports by Dunn et al.,[54] Linnros et al.,[26] Kalkman et al.,[52] Hannah et al.,[12] Liu et al.,[37] Sangghaleh et al.,[27] and Brown et al.[18] In the report by Linnros et al.,[26] samples prepared by implantation (impl) and electrochemical etching (etch) are shown in different colors. Please note that the average lifetimes (eq 4) are plotted here. Theoretical calculation of radiative rates by Delerue et al.[48] and Yassievich et al.[55] and the estimation of radiative lifetimes by Greben et al.[28] are also shown for comparison.

not influenced by small changes in the input data because the data cover a very broad spectral range and because results obtained by using different experimental setups are included. However, when characterizing a single sample using the experimental setup at hand, the uncertainty of the determined k_{QC}^{exp} values is much higher because of varying noise levels[44] and because the characterization of a single sample is unlikely to cover such a broad spectral range as in Figure 1d. As a result of the exponential dependence involved in the fit, the value of the A_{PL} parameter can significantly change (e.g., 2×) with small changes in the fitted k_{QC}. Therefore, for the characterization of a single sample, it is in practice useful to fix k_{QC} at the "ideal" value $k_{QC}^{exp} = 0.2917$ and estimate A_{PL} using

$$\tau_{PL} = A_{PL} \exp\left(-\frac{E_g(\text{eV})}{0.2917}\right) + y_0 \tag{7}$$

Here, the inclusion of a free y_0 parameter can compensate for small deviations from an ideal $1/k_{QC}^{exp}$ slope, which makes the fitted value of A_{PL} more robust. The typical values of y_0 are on the order of 1×10^{-4} of A_{PL}, confirming that the inclusion of this parameter does not distort the fitted values. This approach is applicable, provided that the divergence from the exponential $\tau_{PL}(\lambda)$ trend is not significant. Thus, for example, in our NTP-SiQD:O sample this simple estimation cannot be used. The A_{PL} parameters of the samples under study here determined in this way are listed in Table 1.

Thus, the knowledge of the universal radiative lifetime dependence in SiQDs, τ_{PL}^{ideal}, from Figure 1d and the approach introduced above allows one to make a quantitative estimation of the importance of slow nonradiative pathways in the sample and to estimate the iQY of this slow emission using experimentally simple tools.

3.5. Stretched-Exponential Dispersion Parameter β.

In some reports,[26−28,37] small changes in the β parameter are discussed with regard to the optical performance and properties of a particular sample. However, the determination of the dispersion parameter β is not as straightforward as it might seem, and in our experience, its exact value is highly sensitive to the determination of background and the onset time. The fitted β tends to vary even in one sample measured under the same conditions several times, while the calculated averaged lifetimes τ_{PL} remain the same. As an example of such behavior, we present two fitted β's of sample HSQ-SiQD:C under low and high excitation intensity; see Figure 2a. Both these measurements are associated with the same average lifetime dependence $\tau_{PL}(\lambda)$ from Figure 1d, albeit with a different margins of error, and thus, both these experiments characterize the same physical mechanisms. However, each data set suggests different $\beta(\lambda)$ trends and different β values.

Therefore, an important question is how much error in the determination of the β parameter is connected to the analysis itself in the presence of experimental noise. To address this issue, we introduce a simple procedure, where we synthetically generate a number of PL decays with known characteristics, artificially add defined levels of noise, and then apply a fitting procedure, as described in detail in the Supporting Information (Section S5). In this way, we can compare the correct parameters characterizing the data β_{real} with the fitted ones β_{fit}. Indeed, as presented in Figure S1, our procedure confirms that the fitted β_{fit} parameter of a single selected data set can substantially differ from the correct value β_{real} and the probability of such deviation naturally increases with the increased noise level. In order to quantify such possible deviations, we introduce data-quality parameters of noise-to-signal ratio N/S and data sparsity N^{signal}, as defined in Section S5 in eqs S4 and S5. Both these parameters can be determined using the underlying PL decay curve and the corresponding fit. Using these two parameters, we can then estimate the probability p of a random data set being fitted "incorrectly", or in other words the probability of the fitted β_{fit} falling outside of the $\langle \beta_{real} - 0.05; \beta_{real} + 0.05 \rangle$ interval (or outside of $\langle 0.9; 1 \rangle$ applying a common constraint $\beta < 1$) using eq S8 and parameters from Table S1.

Coming back to Figure 2a, the fit ambiguity parameter p can help us interpret the observed difference as being solely a result of the presence of different levels of noise in the measurement. The lower-excitation-intensity measurement in black has a much higher uncertainty connected with the determination of β ($p \approx 0.1$−0.15) with a clear tendency of the higher-

https://doi.org/10.1021/acs.jpcc.3c05423
J. Phys. Chem. C 2023, 127, 20426−20437

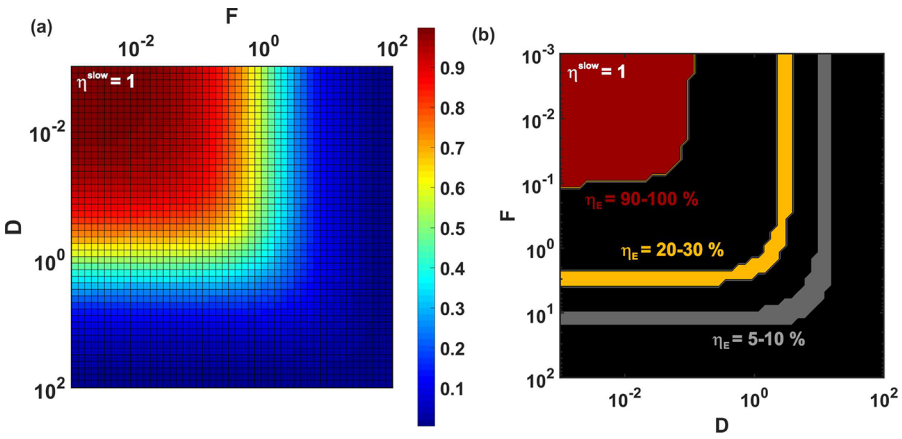

Figure 3. Visualization of eq 10 for $\eta_{slow} = 1$. (a) Influence of the proportion of the dark-to-slow D and the fast-to-slow F subpopulations to the external quantum yield. (b) The colored areas highlight possible combinations of F and D leading to selected quantum yield ranges.

uncertainty data points being fitted with a higher β. Without the information on the uncertainty of the fit, the $\beta(\lambda)$ dependence of this data set could even be interpreted as parabolic (the yellow curve). This hypothesis about a potential parabolic $\beta(\lambda)$ dependence is disproved using higher-quality data (the red curve), which reveal a mostly flat $\beta(\lambda) \approx 0.77$ value (with $p \approx 0.005$).

Therefore, the importance of β should not be overestimated. In our PL decay measurements with high spectral resolution ($\Delta\lambda \approx 5$ nm) and good quality fits (including the onset time and the whole tail of the decay curve, $p \approx 0.02$), the dispersion parameter β is usually in the 0.75−0.85 range when averaged over a wider spectral range and it lacks a clear $\beta(\lambda)$ trend, as in Figure 2a. Values of β close to 0.8 also often appear in the literature in samples with higher quantum yield values (eQY ≈ 20%). On the other hand, the PL decay of "lower-quality" samples (compare, e.g., the two sets of samples reported on by Linnros et al.[26] in Figure 2b) with non-negligible nonradiative pathways tends to be characterized by a lower β around 0.6[26] or even by more complicated decay shapes.[56] Thus, the discussion of the β parameter has its merits, but the limits in its determination due to experimental conditions need to be always considered, and small changes under about 0.1 are more likely a result of experimental noise than an indication of a change in the underlying physics. An example of the application of a data-quality assessment is shown in Section S6, where we show that the PL decays measured in single SiQDs[57] most likely are single exponentials despite the inherent high levels of noise; however, the measured lifetimes are significantly influenced by nonradiative trapping in surrounding SiO_2, in agreement with a follow-up study by the same group.[58]

3.6. External Quantum Yield and Dark Quantum Dots. The slow emission discussed so far is the most common one reported in SiQDs. However, QDs emitting this long-lived PL are not the only subpopulation in an ensemble of SiQDs. Sometimes, another faster blue-shifted PL emission is observed.[14,24,25,59] For the sake of simplicity, we will attribute this emission to a "fast" subpopulation of SiQDs ($\tau_{PL}^{fast} \approx 10$ ns). In addition to light-emitting QDs, a population of "dark" QDs, which absorb the excitation light, but whose emission is zero, are yet another subpopulation of SiQDs with different optical performance.[28,39] Thus, an ensemble of SiQDs can be broken down to (at least) three different QD subpopulations, namely, a "slow", "fast", and "dark" one, with each one being represented as the corresponding relative populations

$$n^{slow} + n^{fast} + n^{dark} = 1 \tag{8}$$

In the samples under study here, the fast blue emission was observed under certain conditions. However, based on our measurements, we concluded that the overall impact of the fast subpopulation on the PL performance of the samples under study here is negligible (not shown). Thus, a more detailed discussion of this fast emission channel is beyond the scope of the current article and will be a topic of a separate report.

The differentiation among these three subpopulation solves the problem of linking the macroscopic QY and the microsopic iQY from eq 3. Within each subpopulation, the QDs are similar enough in their optical performance, and thus we can select a "typical" QD with its own iQY $\eta_{slow/fast}$ in each subpopulation. These iQYs will contribute to the overall eQY as follows:

$$\eta_E = \frac{\sum_j N_{em,j}}{\sum_j N_{abs,j}} = \frac{\sum_j \sigma_j^{exc} n_j \eta_j}{\sum_j \sigma_j^{exc} n_j} = \frac{n^{slow}\eta_{slow} + n^{fast}\eta_{fast}}{n^{slow} + n^{fast} + n^{dark}} \tag{9}$$

where σ^{exc} is the excitation cross-section. Since the excitation occurs to a higher-energy states in SiQDs, we can safely use $\sigma^{exc,fast} \approx \sigma^{exc,slow} \approx \sigma^{exc,dark}$ and, moreover, the n^{dark} subpopulation does not contribute to emission by definition ($n^{dark}\eta_{dark} = 0$). Thus, the eQY formula from eq 2 reduces to the simple weighted sum of the iQYs of the radiatively active subpopulations with the inclusion of dark QDs in the denominator. Due to the overall small contribution of the fast subpopulation to the observed light emission ($\frac{n^{fast}\eta_{fast}}{n^{slow}\eta_{slow}} \ll 1$), eq 9 can be written down simply as

$$\eta_E \approx \frac{\eta_{slow}}{1 + D + F} \approx \frac{\eta_{slow}}{1 + D} \tag{10}$$

where $D = n^{dark}/n^{slow}$ and $F = n^{fast}/n^{slow}$ are the ratios of the subpopulations of dark to slow and fast to slow QDs, respectively.

This simple model visualized in Figure 3 gives us an estimate of how the individual subpopulations influence eQY. In the simplest case if $\eta_{slow} = 1$ and η_{fast} is not too high, it is necessary that both $D < 0.1$ and $F < 0.1$ to obtain a hypothetical ideal sample with $\eta_E \approx 1$. Higher proportions of either the dark D or

https://doi.org/10.1021/acs.jpcc.3c05423
J. Phys. Chem. C 2023, 127, 20426−20437

the fast F subpopulation of 3:1 or 12:1 then lower the eQY to the range of 20−30% and 5−10%, respectively, even if the slow channel is purely radiative ($\eta_{slow} = 1$).

This piece of information is key to understanding the radiative performance. Sometimes, mostly in studies determining the iQY using the Purcell effect, only the slow subpopulation is characterized.[27,32] Indeed, when the iQY of an SiQD ensemble is determined through the Purcell effect or by using the methodology outlined in this article, the determination always relies on microsecond PL decay measurements. Therefore, the n^{dark} (or the fast) subpopulation is omitted and a potential "fully radiative" iQY ≈ 1 result then only signifies the absence of any slow nonradiative channel, without addressing the influence of the dark (or the fast) subpopulation. Despite being a considerable step toward the optimization of SiQD radiative performance, the potential elimination of the slow nonradiative channel might not be the factor determining the overall performance.

Looking at our own results, we can make an estimate, albeit with a considerable margin of error of at least 30%, of the dark-to-slow subpopulation ratio D by combining the approach we use in Section 3.1 and the characterization of eQY and eq 10. The results are listed in Table 1 with the values of D between 2 and 40, which are consistent with the proportion of dark SiQDs in a sample reported elsewhere.[32] The above analysis does not take into account ensemble effects such as energy transfers between the QDs. However, we expect the influence of such effects to be minimal in our measurements, since we use well-dispersed and diluted samples. In matrix-embedded SiQDs, the situation can be different as their eQY depends, among other things, on the thickness of SiO_2 separation layer.[60]

3.7. Factors Influencing Optical Performance. Using all of the information gathered here on the optical performance of the samples under study, we can now assess the influence of various factors on their overall optical performance. We showed that three of the samples, fabricated by synthesis in nonthermal plasma, electrochemical etching and by the disproportionation of HSQ (NTP-SiQD:C, etch-SiQD:Ob, and HSQ-SiQD:C), are fully radiative in the long-lived slow component ($\eta_{slow} \approx 1$; see Figure 1c,d). Two of these samples are dodecyl-passivated (HSQ-SiQD:C and NTP-SiQD:C) and it is obviously the dark subpopulation that lowers their eQY to 26% and 6%, respectively. Thus, in this case, the dark subpopulation is the determining factor. In the sample fabricated by electrochemical etching and subsequently oxidized without the deagglomeration procedure (etch-SiQD:Oa) with lower iQY ($\eta_{slow}^{etch\text{-}SiQD:Oa} \approx 0.2$), the proportion of dark QDs is roughly the same as in the best-performing dodecyl passivated sample HSQ-SiQD:C. In this oxidized sample, the overall eQY is decreased by the slow nonradiative recombination in addition to the dark QDs by a factor of about 4×, implying that this time both the nonradiative pathways and the dark QDs play a significant role. In the electrochemically etched sample which underwent a deagglomeration treatment (etch-SiQD:Ob), the treatment clearly helped curb the slow nonradiative channels, which resulted in fully radiative PL in the slow long-lived component ($\eta_{slow}^{etch\text{-}SiQD:Ob} \approx 1$), but at the same time, the treatment exposed new unpassivated bonds. These new bonds were repassivated, under the conditions of the deagglomeration treatment, in a nonbeneficial way for the overall QY, lowering the eQY through the introduction of dark QDs to the lowest value of all the studied samples.

On the whole, dodecyl-passivated SiQDs have lower amounts of dark QDs, which is in line with the generally higher external quantum efficiencies reported in SiQDs terminated with surface alkyl groups when compared to oxidized SiQDs. Comparing the two dodecyl-capped SiQDs samples in this study, it is even probable that the "type" (activation procedure) of the hydrosilylation can influence D.

4. DISCUSSION

4.1. Importance of Averaged Lifetimes. Based on experimental results, we put forward an emission-photon-energy dependence of radiative lifetimes in the slow channel from Figure 1d as the curve signaling "ideal" long-lived PL lifetimes. The fact that these radiative lifetimes are quantitatively the same regardless of the fabrication method is nontrivial and highlights the generally shared PL properties. The nonstandardized and sometimes even incorrect methods of PL analysis, a problem which we aim to rectify in this article, are one of the reasons why this universality of radiative lifetimes had not been experimentally reported earlier.

In many samples, the measured $\tau_{PL}(\lambda)$ dependence closely matches this ideal radiative curve, implying that the long-lived recombination is fully radiative. The observed $\tau_{PL}^{ideal}(\lambda)$ behavior is universal and is shared by different types of samples (matrix-embedded or oxidized or capped with long alkyls), at least within the margin of experimental error typical for the determination of radiative lifetimes. We want to highlight this striking resemblance, which proves that quantum confinement affects different types of SiQDs in a very similar way. Therefore, the observed universal $\tau_{PL}^{ideal}(\lambda)$ dependence can serve as a benchmark to which the PL dynamics of a newly prepared sample can be compared using relatively standard equipment combined with the proper analysis. We do not *a priori* rule out potential systematic deviations of different types of samples from the observed behavior. However, such potential deviations are the topic for further research, and we propose that they are discussed in relation to this universal framework, which will enable a much more meaningful comparison of the optical performance across different types of SiQDs and in sets of sample where one fabrication parameter is being varied. Moreover, the presented results also do not necessarily imply that the size dependence of the radiative lifetimes $\tau_r(d)$ in all the sample types is the same, because a different type of surface (oxide vs alkyls) or embedding in a matrix[61] can induce shifts in the size dependence of the energy gap.

However, a crucial step in comparing the measured PL decays of different samples is the use of the average lifetime τ_{PL} from eq 5 rather than the typically reported stretched-exponential decay lifetime τ_{SE}. In Section 3.5, we argue that the calculated value of β can be distorted by the noise in the data. In a fitting procedure, both β and τ_{SE} are determined at the same time using a given decay curve, implying that noise levels and data quality influence both of these parameters. In other words, the calculated value of τ_{SE} can also fluctuate solely as a result of noise in the data if the data are of insufficient quality. On the other hand, the average PL lifetime τ_{PL} from eq 5 combining β and τ_{SE} is a much more robust quantity. If the average PL lifetime is plotted, then the resulting trends are no longer sensitive to small changes in noise levels and to the overall quality of the data. This criterion alone confirms that τ_{PL} is indeed a much more appropriate quantity to characterize the PL decay than the combination of (τ_{SE}, β). Last but not

https://doi.org/10.1021/acs.jpcc.3c05423
J. Phys. Chem. C 2023, 127, 20426−20437

least, the τ_{PL} value is independent of the applied decay model, and therefore the results are directly comparable even if the data are fitted as a combination of two or three single exponentials with different lifetimes. Thus, τ_{PL} is especially useful if there is some uncertainty about the PL dynamics and lifetime dispersion in the sample. The usefulness of the τ_{PL} approach is illustrated in Figure 2b, which directly compares the lifetimes reported by independent laboratories on many different types of samples investigated when presented by using the τ_{PL} notation.

Thus, we deem it a good practice to report (i) the average τ_{PL} of an PL decay rather than simply the τ_{SE} parameter, (ii) to discuss the quality of the fit using the fit ambiguity parameter p when addressing any underlying trends, and (iii) to consider only larger changes in the dispersion parameter β using high-quality data ($p < 0.02$). Following this recommended analysis would allow for a much more meaningful comparison of results reported by different laboratories and it would eliminate potential discussions of false trends resulting solely from data treatment.

The methodology we present here is clearly valid generally for any material; however, the materials which would benefit from this approach the most are those which exhibit significant dependence of photoluminescence lifetimes on the emission photon energy, which are typically indirect-bandgap materials. We emphasize that in order for the methodology quantifying the population of dark QDs D to work, the radiative lifetimes of the material need to be determined by accurate methods such as the measurement of the Purcell effect, as we discuss in Section 3.2 for silicon. More generally, the application of average lifetimes from Section S2 and fit quality assessment from Section 3.5 and Section S5 are purely mathematical concepts, and therefore, they are valid regardless of the material under study.

4.2. Fully Radiative PL Decays and Their Stretched-Exponential Character. The PL decay of a single QD is assumed to be single-exponential[48,57] and the non-single-exponential character of ensemble PL is then caused by a dispersion of a property in the ensemble.[18,26,27,62,63] In the long-lived PL of SiQDs, the non-single-exponential character of PL decay is a common occurrence and was observed throughout electrochemically etched SiQDs,[64−68] SiQDs prepared by high-temperature annealing of Si-rich SiO_2 layers,[26,54] and colloidal dodecyl capped SiQDs,[27,28,37,69] even at low temperatures[63] or in size-separated colloidal ensembles.[56] Despite a few exceptions,[28,62] all the SiQDs in the ensemble are often assumed to share exactly the same radiative lifetime value at a given λ and only nonradiative lifetimes are expected to vary on a dot-to-dot basis.[27] Here, we want to highlight the possibility of a different physical model, namely, the variation of the radiative lifetime value in an ensemble of SiQDs on a dot-to-dot basis as an alternative explanation of $\beta < 1$ in fully radiative, and other, samples. Such a distribution of radiative lifetimes, even if it contained only a few values, could naturally explain $\beta < 1$ even if $\eta_{slow} = 1$, which is a situation observed here and elsewhere.[27]

The reason why we expect a natural variation of radiative lifetimes in an ensemble of SiQDs stems from the fact that in reality, a QD is an extremely small crystal in which a large number of structural arrangements of atoms are possible[70] and it is highly likely that more than one type of structural arrangement, which we will refer to as the variations in "shape", will occur in an ensemble. Such structural variations were considered even in theoretical calculations by Delerue et al.,[48] who showed that this variation in shape results in a dispersion in radiative lifetimes. The inclusion of shape variations by Delerue et al.[48] is in contrast to many theoretical reports that only study a predesigned set of QDs differing in size without considering the potential influence of the QD's shape, such as the one by Yassievich et al.[55] Both these calculated trends are compared to "our" ideal $\tau_{PL}^{ideal}(\lambda)$ curve in Figure 2b. Despite the very satisfactory agreement of the PL lifetime values obtained with both these calculations[48,55] and our experimental $\tau_{PL}^{ideal}(\lambda)$ curve, the lifetimes put forward by Yassievich et al.[55] disregarding the possible variation of shapes clearly exhibit a different trend. Thus, including potential shape variations leads to a description that is in better agreement with experimental data, making it much more relevant for experiments. Thus, analogically to the calculation by Delerue et al.,[48] we propose the physical interpretation of the universal $\tau_{PL}^{ideal}(\lambda)$ curve reported on here as a quantification of the optical behavior typical for a large number of QDs when averaged over the whole ensemble even though natural dot-to-dot variations in QD shape and consequently also τ_r are present.

Yet another theoretical assessment of radiative lifetimes in SiQDs supporting the possibility of dot-to-dot variation in τ_r is the phenomenological estimation suggested by Greben et al.,[28] also included in Figure 2b. Here, the radiative lifetimes were calculated using the envelope function approximation, yielding a very good agreement with our proposed $\tau_{PL}^{ideal}(\lambda)$ curve, and the variation in τ_r is explicitly proposed as the most natural explanation of the observed results.

4.3. Other Factors Influencing the Determination of Radiative Lifetimes. There is a small (≈20%) difference in the A_{PL} parameter of the theoretical calculations of radiative rates by Delerue et al.[48] and our proposed $\tau_{PL}^{ideal}(\lambda)$ curve. This difference can be caused by the short-pulsed pulsed excitation typically used to characterize PL decays, which selectively excites only the faster-decaying SiQDs in an ensemble,[53] leading to shorter lifetimes being obtained by the short pulsed excitation than those characterizing the whole ensemble are. (We opt for reporting the lifetimes resulting from the short-pulse excitation rather than a long-pulse one because the short-pulse excitation is the standard method to measure PL decays.) In addition to this size-dispersion factor, the effect of the surrounding medium on the measured lifetimes also needs to be accounted for through the local field factor.[48,53] We do not take this factor into consideration in our analysis, however, the effect of the surrounding medium is already included in all the three theoretical approaches discussed here.[28,48,55]

4.4. Quenching Mechanisms of Dark Quantum Dots. One question that naturally arises at this point is what mechanism quenches the QD's PL and renders it dark. Are the dark QDs a result of the low degree of internal order in the QD's core, or is it the surface passivation where improperly passivated sites act as PL quenching defects? Clearly, we are unable to answer this question at this stage of research; however, we can offer a speculation based on our results. The lowest amount of dark QDs is present in the sample fabricated by electrochemical etching from a highly crystalline Si wafer (etch-SiQD:Oa), immediately suggesting that the quality of the core is a very important factor. However, after a deagglomeration treatment (etch-SiQD:Ob), which influences the surface passivation, this ratio rises considerably, implying that the quality of surface passivation can increase the number

https://doi.org/10.1021/acs.jpcc.3c05423
J. Phys. Chem. C 2023, 127, 20426−20437

of dark QD. The question if the "background" level of D in the QDs prepared from a highly crystalline Si wafer is due to possible imperfections in surface passivation or simply a result of varied shapes of QDs produced by etching cannot be addressed at this point. Both the samples which were fabricated through NTP synthesis, at least in our implementation, and are thus in general more likely to contain structural imperfections, have their D higher than the electrochemically etched one, albeit only to a small degree. This observation would be in line with potential structural factors influencing the dark-to-slow ratio. Thus, most likely both the structural imperfections and suboptimal surface passivation can influence the number of dark QDs and subsequently deteriorate the overall PL performance. In order to shed more light on this problem, a much larger database of fabrication protocols and the corresponding optical performance including D and A_{PL} would be necessary.

5. CONCLUSIONS

Based on a thorough comparison of the PL decays of several types of samples and literature data, we put forward an experimental observation that the typical slow PL decay is often fully radiative in colloidal SiQDs. We propose an ideal dependence of photoluminescence lifetimes on emission photon energy, $\tau_{PL}^{ideal}(\lambda)$, which can be easily applied to other samples in order to quantify potential deviations from this fully radiative behavior. This ideal dependence is universal and is shared by SiQD samples fabricated by different approaches, but it only becomes evident when the average PL lifetimes are compared. Despite the fully radiative PL decay, SiQDs do not exhibit single-exponential PL decay, which we attribute also to a degree of natural variations in radiative lifetimes within the ensemble of QDs. Moreover, we discuss the limitations of the interpretation of the dispersion PL decay parameter β and the stretched-exponential lifetime and a possible overemphasis that is sometimes placed on the β parameter by introducing a measure helping to identify statistically significant trends in collected data.

Even if fully radiative long-lived PL recombination is achieved in SiQDs, the "slow" subpopulation still constitutes only one out of (at least) three subpopulations of QDs in the ensemble. In order to properly characterize and optimize the PL performance of SiQDs, the effect of the other subpopulations also needs to be assessed. Whereas the influence of the fast subpopulation is often negligible, the dark subpopulation can considerably affect the overall PL QY of SiQDs. Using the knowledge of the universal radiative lifetimes and external quantum efficiency, the relative proportion of dark QDs (D = 2−40) in the SiQD samples can be estimated, and its influence of the overall PL performance is discussed. This simple approach provides a methodology for a more in-depth discussion of the influence of the synthesis and surface-passivation methods on the relative population of dark SiQDs in an ensemble and thus the mechanisms responsible for rendering SiQDs dark.

Even if we introduce this methodology for Si QDs, other QDs, notably those with indirect bandgap and emission-photon-energy dependent lifetimes, can benefit from this approach provided that radiative lifetimes are determined using a reliable method. Other purely mathematical concepts, such as the average lifetimes in general or the fit-quality assessment, are obviously applicable regardless of the studied material.

ASSOCIATED CONTENT

Supporting Information

The Supporting Information is available free of charge at https://pubs.acs.org/doi/10.1021/acs.jpcc.3c05423.

Information on the collection and treatment of PL decay data and on the compilation of literature data and description of the average lifetimes and the method used to determine the accuracy of the stretched-exponential fitting parameter (PDF)

AUTHOR INFORMATION

Corresponding Author

Kateřina Kůsová − *Institute of Physics of the ASCR, v.v.i., 162 00 Prague 6, Czechia;* orcid.org/0000-0002-8545-5965; Email: kusova@fzu.cz

Authors

Tomáš Popelář − *Institute of Physics of the ASCR, v.v.i., 162 00 Prague 6, Czechia;* orcid.org/0000-0001-9785-4675

Pavel Galář − *Institute of Physics of the ASCR, v.v.i., 162 00 Prague 6, Czechia;* orcid.org/0000-0003-2220-2976

Filip Matějka − *Institute of Physics of the ASCR, v.v.i., 162 00 Prague 6, Czechia*

Giacomo Morselli − *Chemistry Department "Giacomo Ciamician", Via F. Selmi 2, University of Bologna, 40126 Bologna, Italy;* orcid.org/0000-0001-9113-6381

Paola Ceroni − *Chemistry Department "Giacomo Ciamician", Via F. Selmi 2, University of Bologna, 40126 Bologna, Italy;* orcid.org/0000-0001-8916-1473

Complete contact information is available at: https://pubs.acs.org/10.1021/acs.jpcc.3c05423

Notes

The authors declare no competing financial interest.

ACKNOWLEDGMENTS

The Czech Science Foundation funding, Grant No. 23-05837S (T.P., P.G., F.M., K.K.) is gratefully acknowledged. We also acknowledge Prof. J. Valenta for making the eQY measurements and Prof. I. Pelant for fruitful discussions and going through the manuscript.

REFERENCES

(1) Kovalenko, M. V.; Manna, L.; Cabot, A.; Hens, Z.; Talapin, D. V.; Kagan, C. R.; Klimov, V. I.; Rogach, A. L.; Reiss, P.; Milliron, D. J.; et al. Prospects of Nanoscience with Nanocrystals. *ACS Nano* **2015**, *9*, 1012−1057.

(2) Milliken, S.; Thiessen, A. N.; Cheong, I. T.; O'Connor, K. M.; Li, Z.; Hooper, R. W.; Robidillo, C. J. T.; Veinot, J. G. C. Turning the dials": controlling synthesis, structure, composition, and surface chemistry to tailor silicon nanoparticle properties. *Nanoscale* **2021**, *13*, 16379−16404.

(3) Beri, D. Silicon quantum dots: surface matter, what next? *Mater. Adv.* **2023**, *4*, 3380−3398.

(4) Mazzaro, R.; Romano, F.; Ceroni, P. Long-lived luminescence of silicon nanocrystals: from principles to applications. *Phys. Chem. Chem. Phys.* **2017**, *19*, 26507−26526.

(5) Huang, J.; Zhou, J.; Jungstedt, E.; Samanta, A.; Linnros, J.; Berglund, L. A.; Sychugov, I. Large-Area Transparent "Quantum Dot Glass" for Building-Integrated Photovoltaics. *ACS Photonics* **2022**, *9*, 2499−2509.

(6) Mazzaro, R.; Gradone, A.; Angeloni, S.; Morselli, G.; Cozzi, P. G.; Romano, F.; Vomiero, A.; Ceroni, P. Hybrid Silicon Nanocrystals

for Color-Neutral and Transparent Luminescent Solar Concentrators. *ACS Photonics* **2019**, *6*, 2303−2311.
(7) Yang, D.; Cui, Z.; Wen, Z.; Piao, Z.; He, H.; Wei, X.; Wang, L.; Mei, S.; Zhang, W.; Guo, R. Recent Updates on Functionalized Silicon Quantum-Dot-Based Nanoagents for Biomedical Applications. *ACS Mater. Lett.* **2023**, *5*, 985−1008.
(8) Romano, F.; Angeloni, S.; Morselli, G.; Mazzaro, R.; Morandi, V.; Shell, J. R.; Cao, X.; Pogue, B. W.; Ceroni, P. Water-soluble silicon nanocrystals as NIR luminescent probes for time-gated biomedical imaging. *Nanoscale* **2020**, *12*, 7921−7926.
(9) Hybertsen, M. S. Absorption and Emission of Light in Nanoscale Silicon Structures. *Phys. Rev. Lett.* **1994**, *72*, 1514−1517.
(10) Kovalev, D.; Heckler, H.; Ben-Chorin, M.; Polisski, G.; Schwartzkopff, M.; Koch, F. Breakdown of the *k*-Conservation Rule in Si Nanocrystals. *Phys. Rev. Lett.* **1998**, *81*, 2803−2806.
(11) Sychugov, I.; Valenta, J.; Mitsuishi, K.; Fujii, M.; Linnros, J. Photoluminescence measurements of zero-phonon optical transitions in silicon nanocrystals. *Phys. Rev. B* **2011**, *84*, 125326.
(12) Hannah, D. C.; Yang, J.; Podsiadlo, P.; Chan, M. K. Y.; Demortiére, A.; Gosztola, D. J.; Prakapenka, V. B.; Schatz, G. C.; Kortshagen, U.; Schaller, R. D. On the Origin of Photoluminescence in Silicon Nanocrystals: Pressure-Dependent Structural and Optical Studies. *Nano Lett.* **2012**, *12*, 4200−4205.
(13) Hapala, P.; Kůsová, K.; Pelant, I.; Jelínek, P. Theoretical analysis of electronic band structure of 2- to 3-nm Si nanocrystals. *Phys. Rev. B* **2013**, *87*, 195420.
(14) Pringle, T. A.; Hunter, K. I.; Brumberg, A.; Anderson, K. J.; Fagan, J. A.; Thomas, S. A.; Petersen, R. J.; Sefannaser, M.; Han, Y.; Brown, S. L.; et al. Bright Silicon Nanocrystals from a Liquid Precursor: Quasi-Direct Recombination with High Quantum Yield. *ACS Nano* **2020**, *14*, 3858−3867.
(15) Canham, L. Introductory lecture: origins and applications of efficient visible photoluminescence from silicon-based nanostructures. *Faraday Discuss.* **2020**, *222*, 10−81.
(16) Dohnalová, K.; Kůsová, K. In *Silicon Photonics IV. Topics in Applied Physics*; Lockwood, D., Pavesi, L., Eds.; Springer Nature: Cham, Switzerland, 2021; Vol. *139*, Chapter 1, pp 3−65.
(17) Dasog, M.; Yang, Z.; Regli, S.; Atkins, T. M.; Faramus, A.; Singh, M. P.; Muthuswamy, E.; Kauzlarich, S. M.; Tilley, R. D.; Veinot, J. G. C. Chemical Insight into the Origin of Red and Blue Photoluminescence Arising from Freestanding Silicon Nanocrystals. *ACS Nano* **2013**, *7*, 2676−2685.
(18) Brown, S. L.; Miller, J. B.; Anthony, R. J.; Kortshagen, U. R.; Kryjevski, A.; Hobbie, E. K. Abrupt Size Partitioning of Multimodal Photoluminescence Relaxation in Monodisperse Silicon Nanocrystals. *ACS Nano* **2017**, *11*, 1597−1603.
(19) Carroll, G. M.; Limpens, R.; Neale, N. R. Tuning Confinement in Colloidal Silicon Nanocrystals with Saturated Surface Ligands. *Nano Lett.* **2018**, *18*, 3118−3124.
(20) Oliinyk, B. V.; Korytko, D.; Lysenko, V.; Alekseev, S. Are Fluorescent Silicon Nanoparticles Formed in a One-Pot Aqueous Synthesis? *Chem. Mater.* **2019**, *31*, 7167−7172.
(21) Thiessen, A. N.; Zhang, L.; Oliynyk, A. O.; Yu, H.; O'Connor, K. M.; Meldrum, A.; Veinot, J. G. C. A Tale of Seemingly "Identical" Silicon Quantum Dot Families: Structural Insight into Silicon Quantum Dot Photoluminescence. *Chem. Mater.* **2020**, *32*, 6838−6846.
(22) Yu, Y.; Fan, G.; Fermi, A.; Mazzaro, R.; Morandi, V.; Ceroni, P.; Smilgies, D.-M.; Korgel, B. A. Size-Dependent Photoluminescence Efficiency of Silicon Nanocrystal Quantum Dots. *J. Phys. Chem. C* **2017**, *121*, 23240−23248.
(23) Dohnalová, K.; Gregorkiewicz, T.; Kůsová, K. Silicon quantum dots: surface matters. *J. Phys.:Condens. Matter.* **2014**, *26*, 173201.
(24) Galář, P.; Popelář, T.; Khun, J.; Matulková, I.; Němec, I.; Newell, K.; Michalcová, A.; Scholtz, V.; Kůsová, K. The red and blue luminescence in silicon nanocrystals with oxidized, nitrogen-containing shell. *Faraday Discuss.* **2020**, *222*, 240−257.
(25) Ondič, L.; Kůsová, K.; Ziegler, M.; Fekete, L.; Gärtnerová, V.; Cháb, V.; Holý, V.; Cibulka, O.; Herynková, K.; Gallart, M.; et al. A complex study of the fast blue luminescence of oxidized silicon nanocrystals: the role of the core. *Nanoscale* **2014**, *6*, 3837−3845.
(26) Linnros, J.; Lalic, N.; Galeckas, A.; Grivickas, V. Analysis of the Stretched Exponential Photoluminescence Decay from Nanometer-sized Silicon Crystals in SiO_2. *J. Appl. Phys.* **1999**, *86*, 6128.
(27) Sangghaleh, F.; Sychugov, I.; Yang, Z.; Veinot, J. G. C.; Linnros, J. Near-Unity Internal Quantum Efficiency of Luminescent Silicon Nanocrystals with Ligand Passivation. *ACS Nano* **2015**, *9*, 7097−7104.
(28) Greben, M.; Khoroshyy, P.; Liu, X.; Pi, X.; Valenta, J. Fully radiative relaxation of silicon nanocrystals in colloidal ensemble revealed by advanced treatment of decay kinetics. *J. Appl. Phys.* **2017**, *122*, 034304.
(29) Greben, M.; Khoroshyy, P.; Sychugov, I.; Valenta, J. Non-exponential decay kinetics: correct assessment and description illustrated by slow luminescence of Si nanostructures. *Appl. Spectr. Rev.* **2019**, *54*, 758−801.
(30) Miura, S.; Nakamura, T.; Fujii, M.; Inui, M.; Hayashi, S. Size dependence of photoluminescence quantum efficiency of Si nanocrystals. *Phys. Rev. B* **2006**, *73*, 245333.
(31) Walters, R. J.; Kalkman, J.; Polman, A.; Atwater, H. A.; de Dood, M. J. A. Photoluminescence quantum efficiency of dense silicon nanocrystal ensembles in SiO_2. *Phys. Rev. B* **2006**, *73*, 132302.
(32) Valenta, J.; Greben, M.; Dyakov, S. A.; Gippius, N. A.; Hiller, D.; Gutsch, S.; Zacharias, M. Nearly perfect near-infrared luminescence efficiency of Si nanocrystals: A comprehensive quantum yield study employing the Purcell effect. *Sci. Rep.* **2019**, *9*, 11214.
(33) van Dam, B.; Osorio, C. I.; Hink, M. A.; Muller, R.; Koenderink, A. F.; Dohnalova, K. High Internal Emission Efficiency of Silicon Nanoparticles Emitting in the Visible Range. *ACS Photonics* **2018**, *5*, 2129−2136.
(34) Valenta, J. Determination of absolute quantum yields of luminescing nanomaterials over a broad spectral range: from the integrating sphere theory to the correct methodology. *Nanoscience Methods* **2014**, *3*, 11−27.
(35) Van Dam, B.; Bruhn, B.; Dohnal, G.; Dohnalová, K. Limits of emission quantum yield determination. *AIP Adv.* **2018**, *8*, 085313.
(36) Mastronardi, M. L.; Maier-Flaig, F.; Faulkner, D.; Henderson, E. J.; Kübel, C.; Lemmer, U.; Ozin, G. A. Size-Dependent Absolute Quantum Yields for Size-Separated Colloidally-Stable Silicon Nanocrystals. *Nano Lett.* **2012**, *12*, 337−342.
(37) Liu, X.; Zhang, Y.; Yu, T.; Qiao, X.; Gresback, R.; Pi, X.; Yang, D. Optimum Quantum Yield of the Light Emission from 2 to 10 nm Hydrosilylated Silicon Quantum Dots. *Part. Part. Syst. Char.* **2016**, *33*, 44−52.
(38) Maier-Flaig, F.; Henderson, E. J.; Valouch, S.; Klinkhammer, S.; Kübel, C.; Ozin, G. A.; Lemmer, U. Photophysics of organically-capped silicon nanocrystals - A closer look into silicon nanocrystal luminescence using low temperature transient spectroscopy. *Chem. Phys.* **2012**, *405*, 175−180.
(39) Limpens, R.; Gregorkiewicz, T. Spectroscopic investigations of dark Si nanocrystals in SiO_2 and their role in external quantum efficiency quenching. *J. Appl. Phys.* **2013**, *114*, 074304.
(40) Galář, P.; Stuchlík, J.; Müller, M.; Kočka, J.; Kůsová, K. Highly spherical SiC nanoparticles grown in nonthermal plasma. *Plasma Process Polym.* **2022**, *19*, e2100127.
(41) Mazzaro, R.; Gradone, A.; Angeloni, S.; Morselli, G.; Cozzi, P. G.; Romano, F.; Vomiero, A.; Ceroni, P. Hybrid Silicon Nanocrystals for Color-Neutral and Transparent Luminescent Solar Concentrators. *ACS Photonics* **2019**, *6*, 2303−2311.
(42) Dohnalová, K.; Ondič, L.; Kůsová, K.; Pelant, I.; Rehspringer, J. L.; Mafouana, R.-R. White-Emitting Oxidized Silicon Nanocrystals: Discontinuity in Spectral Development with Reducing Size. *J. Appl. Phys.* **2010**, *107*, 053102.
(43) Zajac, V.; Němec, H.; Kadlec, C.; Kůsová, K.; Pelant, I.; Kužel, P. THz photoconductivity in light-emitting surface-oxidized Si nanocrystals: the role of large particles. *New J. Phys.* **2014**, *16*, 093013.

(44) Kůsová, K.; Popelář, T. On the importance of onset times and multiple-wavelength analysis of photoluminescence decays. *J. Appl. Phys.* **2019**, *125*, 193103.
(45) Wang, Y.; Townsend, P. Potential problems in collection and data processing of luminescence signals. *J. Lumin.* **2013**, *142*, 202−211.
(46) Lemmetyinen, H.; Tkachenko, N. V.; Valeur, B.; Hotta, J.-i.; Ameloot, M.; Ernsting, N. P.; Gustavsson, T.; Boens, N. Time-resolved fluorescence methods (IUPAC Technical Report). *Pure Appl. Chem.* **2014**, *86*, 1969−1998.
(47) Kůsová, K.; Popelář, T.; Pelant, I.; Morselli, G.; Angeloni, S.; Ceroni, P. Trap-State-Induced Becquerel Type of Photoluminescence Decay in DPA-Activated Silicon Nanocrystals. *J. Phys. Chem. C* **2021**, *125*, 2055−2063.
(48) Delerue, C.; Allan, G.; Reynaud, C.; Guillois, O.; Ledoux, G.; Huisken, F. Multiexponential photoluminescence decay in indirect-gap semiconductor nanocrystals. *Phys. Rev. B* **2006**, *73*, 235318.
(49) Delerue, C.; Allan, G.; Lannoo, M. Theoretical aspects of the luminescence of porous silicon. *Phys. Rev. B* **1993**, *48*, 11024−11036.
(50) Greben, M.; Khoroshyy, P.; Gutsch, S.; Hiller, D.; Zacharias, M.; Valenta, J. Changes of the absorption cross section of Si nanocrystals with temperature and distance. *Beilstein J. Nanotechnol.* **2017**, *8*, 2315−2323.
(51) De Jong, E. M.; Rutjes, H.; Valenta, J.; Trinh, M. T.; Poddubny, A. N.; Yassievich, I. N.; Capretti, A.; Gregorkiewicz, T. Thermally stimulated exciton emission in Si nanocrystals. *Light Sci. Appl.* **2018**, *7*, 17133−17137.
(52) Kalkman, J.; Gersen, H.; Kuipers, L.; Polman, A. Excitation of surface plasmons at a SiO_2Ag interface by silicon quantum dots: Experiment and theory. *Phys. Rev. B* **2006**, *73*, 075317.
(53) Greben, M.; Valenta, J. Note: On the choice of the appropriate excitation-pulse-length for assessment of slow luminescence decays. *Rev. Sci. Instrum.* **2016**, *87*, 126101.
(54) Dunn, K.; Derr, J.; Johnston, T.; Chaker, M.; Rosei, F. Multiexponential photoluminescence decay of blinking nanocrystal ensembles. *Phys. Rev. B* **2009**, *80*, 035330.
(55) Yassievich, I. N.; Moskalenko, A. S.; Prokofiev, A. A. Confined electrons and holes in Si nanocrystals: Theoretical modeling of the energy spectrum and radiative transitions. *Mater. Sci. Eng., C* **2007**, *27*, 1386−1389.
(56) Brown, S. L.; Krishnan, R.; Elbaradei, A.; Sivaguru, J.; Sibi, M. P.; Hobbie, E. K. Origin of stretched-exponential photoluminescence relaxation in size-separated silicon nanocrystals. *AIP Adv.* **2017**, *7*, 055314.
(57) Sangghaleh, F.; Bruhn, B.; Schmidt, T.; Linnros, J. Exciton lifetime measurements on single silicon quantum dots. *Nanotechnology* **2013**, *24*, 225204.
(58) Pevere, F.; Sangghaleh, F.; Bruhn, B.; Sychugov, I.; Linnros, J. Rapid trapping as the origin of nonradiative recombination in semiconductor nanocrystals. *ACS Photonics* **2018**, *5*, 2990−2996.
(59) de Boer, W. D. A. M.; Timmerman, D.; Dohnalova, K.; Yassievich, I. N.; Zhang, H.; Buma, W. J.; Gregorkiewicz, T. Red spectral shift and enhanced quantum efficiency in phonon-free photoluminescence from silicon nanocrystals. *Nat. Nanotechnol.* **2010**, *5*, 878−884.
(60) Valenta, J.; Greben, M.; Gutsch, S.; Hiller, D.; Zacharias, M. Photoluminescence performance limits of Si nanocrystals in silicon oxynitride matrices. *J. Appl. Phys.* **2017**, *122*, 144303.
(61) Kůsová, J.; Ondič, J.; Klimešová, J.; Herynková, J.; Pelant, J.; Daniš, J.; Valenta, J.; Gallart, J.; Ziegler, J.; Hönerlage, J.; et al. Luminescence of free-standing versus matrix-embedded oxide-passivated silicon nanocrystals: the role of matrix-induced strain. *Appl. Phys. Lett.* **2012**, *101*, 143101.
(62) Guillois, O.; Herlin-Boime, N.; Reynaud, C.; Ledoux, G.; Huisken, F. Photoluminescence decay dynamics of noninteracting silicon nanocrystals. *J. Appl. Phys.* **2004**, *95*, 3677−3682.
(63) Pavesi, L. Influence of dispersive exciton motion on the recombination dynamics in porous silicon. *J. Appl. Phys.* **1996**, *80*, 216−225.
(64) Vial, J. C.; Bsiesy, A.; Gaspard, F.; Herino, R.; Ligeon, M.; Muller, F.; Romestain, R.; Macfarlane, R. M. Mechanisms of visible-light emission from electro-oxidized porous silicon. *Phys. Rev. B* **1992**, *45*, 14171−14176.
(65) Chen, X.; Henderson, B.; O'Donnell, K. P. Luminescence decay in disordered low-dimensional semiconductors. *Appl. Phys. Lett.* **1992**, *60*, 2672−2674.
(66) Mihalcescu, I.; Vial, J. C.; Romestain, R. Carrier localization in porous silicon investigated by time-resolved luminescence analysis. *J. Appl. Phys.* **1996**, *80*, 2404.
(67) Pavesi, L.; Ceschini, M. Stretched-exponential decay of the luminescence in porous silicon. *Phys. Rev. B* **1993**, *48*, 17625−17628.
(68) Xie, Y. H.; Wilson, W. L.; Ross, F. M.; Mucha, J. A.; Fitzgerald, E. A.; Macaulay, J. M.; Harris, T. D. Luminescence and structural study of porous silicon films. *J. Appl. Phys.* **1992**, *71*, 2403−2407.
(69) Li, Z.; Kortshagen, U. R. Aerosol-Phase Synthesis and Processing of Luminescent Silicon Nanocrystals. *Chem. Mater.* **2019**, *31*, 8451−8458.
(70) König, D. Number series of atoms, interatomic bonds and interface bonds defining zinc-blende nanocrystals as function of size, shape and surface orientation: Analytic tools to interpret solid state spectroscopy data. *AIP Adv.* **2016**, *6*, 085306.

https://doi.org/10.1021/acs.jpcc.3c05423
J. Phys. Chem. C 2023, 127, 20426−20437